Journal of Dental Research
2021, Vol. 100(6) 639–647

DOI: 10.1177/0022034520981854
journals.sagepub.com/home/jdr

Ablation of Pyrophosphate Regulators Promotes Periodontal Regeneration

A. Nagasaki[1], K. Nagasaki[1], E.Y. Chu[1], B.D. Kear[1], W.D. Tadesse[1], S.E. Ferebee[1], L. Li[2], B.L. Foster[3], and M.J. Somerman[1]

Abstract

Biomineralization is regulated by inorganic pyrophosphate (PP_i), a potent physiological inhibitor of hydroxyapatite crystal growth. Progressive ankylosis protein (ANK) and ectonucleotide pyrophosphatase/phosphodiesterase 1 (ENPP1) act to increase local extracellular levels of PP_i, inhibiting mineralization. The periodontal complex includes 2 mineralized tissues, cementum and alveolar bone (AB), both essential for tooth attachment. Previous studies demonstrated that loss of function of ANK or ENPP1 (reducing PP_i) resulted in increased cementum formation, suggesting PP_i metabolism may be a target for periodontal regenerative therapies. To compare the effects of genetic ablation of *Ank, Enpp1*, and both factors concurrently on cementum and AB regeneration, mandibular fenestration defects were created in *Ank* knockout (*Ank* KO), *Enpp1* mutant (*Enpp1*$^{asj/asj}$), and double KO (dKO) mice. Genetic ablation of *Ank, Enpp1*, or both factors increased cementum regeneration compared to controls at postoperative days (PODs) 15 and 30 (*Ank* KO: 8-fold, 3-fold; *Enpp1*$^{asj/asj}$: 7-fold, 3-fold; dKO: 11-fold, 4-fold, respectively) associated with increased fluorochrome labeling and expression of mineralized tissue markers, dentin matrix protein 1 (*Dmp1*/DMP1), osteopontin (*Spp1*/OPN), and bone sialoprotein (*Ibsp*/BSP). Furthermore, dKO mice featured increased cementum thickness compared to single KOs at POD15 and *Ank* KO at POD30. No differences were noted in AB volume between genotypes, but osteoblast/osteocyte markers were increased in all KOs, partially mineralized osteoid volume was increased in dKO versus controls at POD15 (3-fold), and mineral density was decreased in *Enpp1*$^{asj/asj}$ and dKOs at POD30 (6% and 9%, respectively). Increased numbers of osteoclasts were present in regenerated AB of all KOs versus controls. These preclinical studies suggest PP_i modulation as a potential and novel approach for cementum regeneration, particularly targeting ENPP1 and/or ANK. Differences in cementum and AB regeneration in response to reduced PP_i conditions highlight the need to consider tissue-specific responses in strategies targeting regeneration of the entire periodontal complex.

Keywords: biomineralization, cementogenesis, bone regeneration, periodontium, extracellular matrix, osteoclast

Introduction

Periodontal disease affects approximately 45% of US adults and 20% to 50% of the global population, featuring destruction of tooth root cementum, periodontal ligament (PDL), and alveolar bone, leading to early tooth loss in advanced cases (Kassebaum et al. 2014; Eke et al. 2016). Cementum, located along the tooth root, includes acellular cementum at the cervical aspect and cellular cementum at the apical aspect. Acellular cementum is critical for PDL attachment to the tooth root, while cellular cementum is believed to adjust posteruption tooth position (Bosshardt 2005; Foster et al. 2007; Yamamoto et al. 2010). Although several studies provide data on factors important for periodontal regeneration, existing regenerative therapies are unpredictable, and cementum is especially challenging to regenerate due to gaps in knowledge about cementum formation (Bosshardt 2005; Foster et al. 2007).

Biomineralization is regulated by the ratio of inorganic phosphate (P_i), a component of hydroxyapatite (HA) mineral, to inorganic pyrophosphate (PP_i), a physiological inhibitor of HA formation (Orriss et al. 2016; Chande and Bergwitz 2018). PP_i regulators include progressive ankylosis protein (ANK: *Ank* in mice and *ANKH* in humans), a transmembrane protein that regulates PP_i transport; ectonucleotide pyrophosphatase phosphodiesterase 1 (ENPP1: *Enpp1*), an ecto-enzyme that generates extracellular PP_i from nucleotides; and tissue-non-specific alkaline phosphatase (TNAP: *Alpl*), an ecto-enzyme that hydrolyzes PP_i to P_i (Ho et al. 2000; Rutsch et al. 2003;

[1]Laboratory of Oral Connective Tissue Biology, National Institute of Arthritis and Musculoskeletal and Skin Diseases (NIAMS), National Institutes of Health (NIH), Bethesda, MD, USA
[2]Craniofacial and Skeletal Diseases Branch, National Institute of Dental and Craniofacial Research (NIDCR), National Institutes of Health (NIH), Bethesda, MD, USA
[3]Biosciences Division, College of Dentistry, The Ohio State University, Columbus, OH, USA

A supplemental appendix to this article is available online.

Corresponding Author:
A. Nagasaki, Laboratory of Oral Connective Tissue Biology, National Institute of Arthritis and Musculoskeletal and Skin Diseases (NIAMS), National Institutes of Health (NIH), 9000 Rockville Pike, Building 50, Room 4120, Bethesda, MD 20892, USA.
Email: atsuhiro.nagasaki@nih.gov

Millan 2006; Szeri et al. 2020). Our group and others have shown that factors controlling P_i/PP_i levels play significant roles in the formation of acellular cementum and alveolar bone. Previous studies indicate that loss of either ANK or ENPP1 (increasing extracellular P_i/PP_i ratio) results in a striking hypercementosis phenotype, while loss of TNAP (decreasing extracellular P_i/PP_i ratio) results in minimal cementum formation (Nociti et al. 2002; Foster et al. 2012; Thumbigere-Math et al. 2018; Chu et al. 2020).

Insights into the important role of P_i/PP_i ratio in directing cementum formation prompted us to investigate the potential for P_i/PP_i modulation to promote periodontal regeneration. In a proof-of-principle pilot study using a fenestration periodontal defect model, increased P_i/PP_i ratio increased cementum formation in *Ank* knockout (KO) versus control mice (Rodrigues et al. 2011). This study did not address bone regeneration. Recognizing differences between bone and cementum in response to loss of *Ank* versus *Enpp1* during development, parallel assessment of alveolar bone and cementum regenerative capabilities is imperative. The expanded studies here address important gaps in knowledge, including a direct comparison of cementum regeneration under the influence of genetic ablation of *Ank* versus *Enpp1* or concurrent deletion of both factors, using a mouse fenestration defect model. For the first time, we contrast effects on cementum versus alveolar bone regeneration in response to reduced PP_i concentrations. These data provide insights for strategies to promote regeneration of the periodontal complex.

Materials and Methods

Animals

Animal procedures were performed in accordance with guidelines of the Animal Care and Use Committee (ACUC), National Institutes of Health (NIH). Mice were maintained on a C57BL/6 background and fed a normal rodent diet (NIH-31). Preparation and genotyping of mice were described (Chu et al. 2020). Mice double heterozygote (dHet) for *Ank* and *Enpp1* were bred to produce homozygote *Ank* KO and *Enpp1*$^{asj/asj}$ mice, double-deficient (dKO) mice, and littermate wild-type (WT) or dHet mice were used as controls (Control).

Fenestration Defects

A modified fenestration root surface defect model was used to remove alveolar bone and acellular cementum, as detailed in Appendix Figure 1A (King et al. 1997; Rodrigues et al. 2011). Surgeries were performed on 5-wk-old mice. Mandibles were harvested for analysis at postoperative days (PODs) 15 and 30 (n = 4 mice/genotype at POD15 and POD30 for micro–computed tomography [CT] and histology; n = 3 to 4 mice/genotype at POD30 for double fluorochrome labeling). Male and female mice were combined because no significant sex-related differences in cementum or alveolar bone were noted in a previous study (Chu et al. 2020).

Micro-CT

Mandibles were fixed in 10% formalin for 48 h at room temperature and scanned in 70% ethanol in a μCT 50 (ScancoMedical) at 70 kVp, 85 μA, 0.5-mm Al filter, 900-ms integration time, and 6-μm voxel size. Samples were analyzed using a combination of semiautomatic and manual methods with AnalyzePro 1.0 (AnalyzeDirect), as detailed in the Appendix.

Histology

After micro-CT analyses, mandibles were demineralized in an acetic acid, formalin, and sodium chloride (AFS) solution for 4 wk, as described (Ao et al. 2017). Mandibles were embedded in paraffin for 5-μm serial section and analyzed by hematoxylin and eosin (H&E), in situ hybridization (ISH), immunohistochemistry (IHC), and tartrate-resistant acid phosphatase (TRAP) as described (Ao et al. 2017; Chu et al. 2020). Double fluorochrome labeling using calcein and alizarin red was performed, as described in the Appendix. Regenerated cementum thickness and proportion of root coverage (PRC; %) were measured by H&E staining (Appendix Fig. 1B). For measurement of positive ISH staining, regenerated cementum and alveolar bone were selected in each section under 200× magnification and measured using ImageJ (NIH), as shown in Appendix Figure 2. To count $TRAP^+$ and cathepsin K^+ cells, the wound-healing area was selected, as detailed in the Appendix and Appendix Figure 3.

Statistical Analysis

Results (mean ± SD) were analyzed with Student's t test for independent samples or 1-way analysis of variance followed by Tukey's post hoc test for pairwise comparisons (GraphPad Prism 7; GraphPad Software). Values of $P < 0.05$ were considered statistically significant.

Results

Increased and Additive Cementum Regeneration with Loss of ANK and/or ENPP1

First, cementum regeneration was evaluated. Cementum thickness was measured at 3 points within the fenestration defect: mesial (M), central (C), and distal (D), and PRC was determined. Representative histological images of specimens obtained at POD15 and POD30 are shown in Figure 1A. The 3 KO models showed significantly increased regenerated cementum versus control mice at both POD15 and POD30 (*Ank* KO: 8-fold and 3-fold; *Enpp1*$^{asj/asj}$: 7-fold and 3-fold; dKO: 11-fold and 4-fold, respectively; POD15: $P < 0.01$, POD30: $P < 0.001$). Regenerated cementum in all 3 KO models had cellular inclusions as reported in developmental studies of these KO models (Chu et al. 2020). Importantly, ankylosis was never observed in any of these KOs, consistent

with previous studies (Rodrigues et al. 2011; Wolf et al. 2018; Chu et al. 2020). At POD15, dKO mice showed increased cementum thickness at all points versus single KO mice (dKO vs. *Ank* KO at 1.4-fold; dKO vs. *Enpp1*$^{asj/asj}$ at 1.7-fold, $P < 0.05$), although there were no significant differences between single KOs. Some differences were observed between KO models at selected locations or time points. At POD30, cementum thickness was greater in *Enpp1*$^{asj/asj}$ versus *Ank* KO mice at the distal point (1.2-fold, $P < 0.01$). In addition, dKO cementum was significantly increased versus *Ank* KO at all 3 locations at both POD15 and POD30 (1.4-fold, $P < 0.05$). No differences were observed between dKO and *Enpp1*$^{asj/asj}$ mice at POD30. PRC was increased in *Ank* KO, *Enpp1*$^{asj/asj}$, and dKO mice versus controls ($P < 0.01$), with no differences between KOs. These findings indicate loss of function of ANK and ENPP1 has additive effects on cementum regeneration at an early stage, with loss of ENPP1 activity exhibiting a greater effect on cementum regeneration than loss of ANK.

Cementum regeneration was assessed further by double fluorochrome labeling using calcein and alizarin red injections (injected at POD7 and POD14, respectively). Calcein labeling had similar intensity in all genotypes, while alizarin red exhibited greater intensity in all 3 KO models versus controls, suggestive of rapid mineral deposition (Fig. 1B).

To confirm the identity of regenerated tissue and provide insights into the regenerative cellular response, ISH and IHC were used to assay expression of 3 cementoblast markers, bone sialoprotein (*Ibsp*/BSP), osteopontin (*Spp1*/OPN), and dentin matrix protein (*Dmp1*/DMP1). Stronger expression of transcripts for *Dmp1, Spp1*, and *Ibsp* were observed in root-lining cells of *Ank* KO, *Enpp1*$^{asj/asj}$, and dKO mice at POD15, with continued strong expression at POD30, versus minimal signals in control mice (Fig. 2A). Quantitative measurement of ISH staining area along healing root surfaces indicated these 3 markers were significantly increased in all KO versus controls at both time points ($P < 0.01$) (Fig. 2B). Some differences were observed between single KO and dKO at POD30. *Dmp1* and *Spp1* expression was increased in dKO versus *Enpp1*$^{asj/asj}$ and *Ank* KO mice, respectively (1.7-fold and 1.5-fold, respectively; $P < 0.05$). Comparable results were noted by IHC. OPN robustly immunolocalized to the new cementum in *Ank* KO, *Enpp1*$^{asj/asj}$, and dKO mice, with more modest immunostaining for DMP1 and BSP. Control mice exhibited minimal staining for OPN on root surfaces and no detectable DMP1 or BSP.

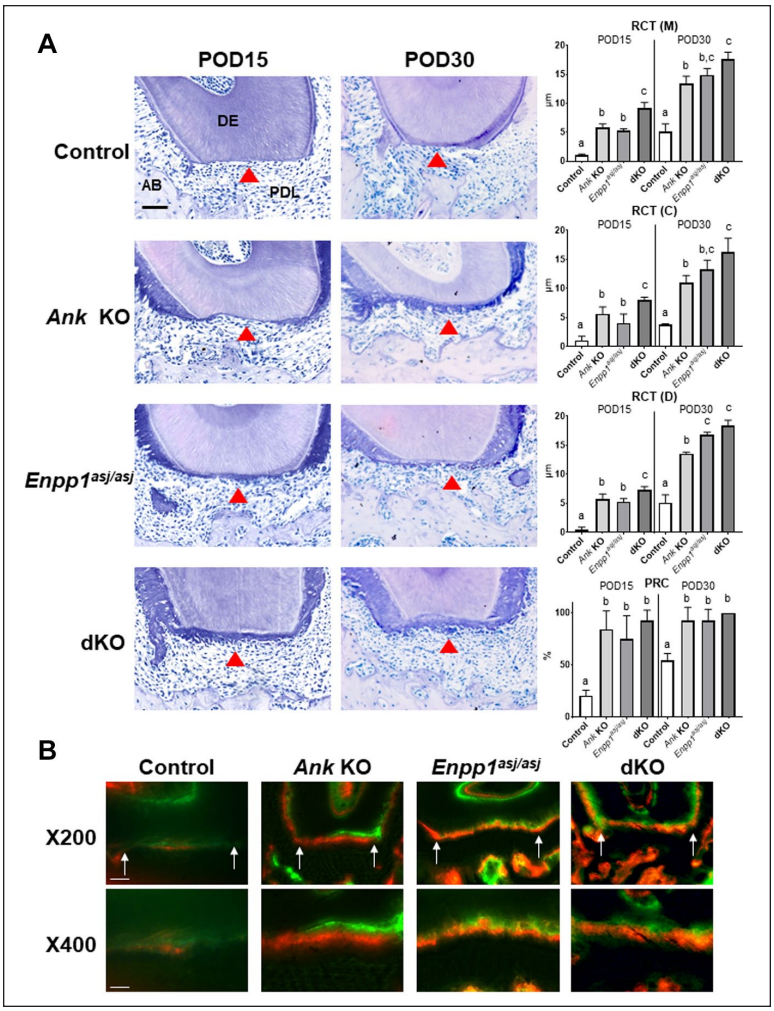

Figure 1. Increased cementum regeneration in *Ank* knockout (KO), *Enpp1*$^{asj/asj}$, and double knockout (dKO) mice. (**A**) Representative images of distal root of first molars at postoperative days (PODs) 15 and 30 ($n = 4$ per genotype). Arrowhead, regenerated cementum; AB, alveolar bone; DE, dentin; PDL, periodontal ligament. Scale bar: 50 µm. Regenerated cementum thickness (RCT) was measured at 3 locations on the distal root of first molars: mesial (M), center (C), and distal (D). The proportion of root coverage (PRC) was measured in wild-type (WT)/dHet, *Ank* KO, *Enpp1*$^{asj/asj}$, and dKO. Experimental groups marked by different letters (a, b, or c) within POD15 or POD30 are significantly different ($P < 0.01$, by one-way analysis of variance), while groups sharing the same letter are not different ($P > 0.05$). (**B**) Double fluorochrome labeling by injection of calcein (green) at POD7 and alizarin red (red) at POD14 (tissues harvested at POD30) reveals new cementum apposition. Arrows indicate wound boundaries. Scale bar: 50 µm in 200× and 25 µm in 400×.

Increased Osteoid Volume and Bone Marker Expression in Alveolar Bone of KO and dKO Mice

Quantity and quality of regenerated alveolar bone were evaluated by micro-CT analysis (Fig. 3A). No differences were noted in regenerated bone volume between any genotypes at POD15 or POD30 (Fig. 3B). Partially mineralized osteoid (i.e., incompletely mineralized bone matrix) was identified based on anatomical location and quantified using a lower density

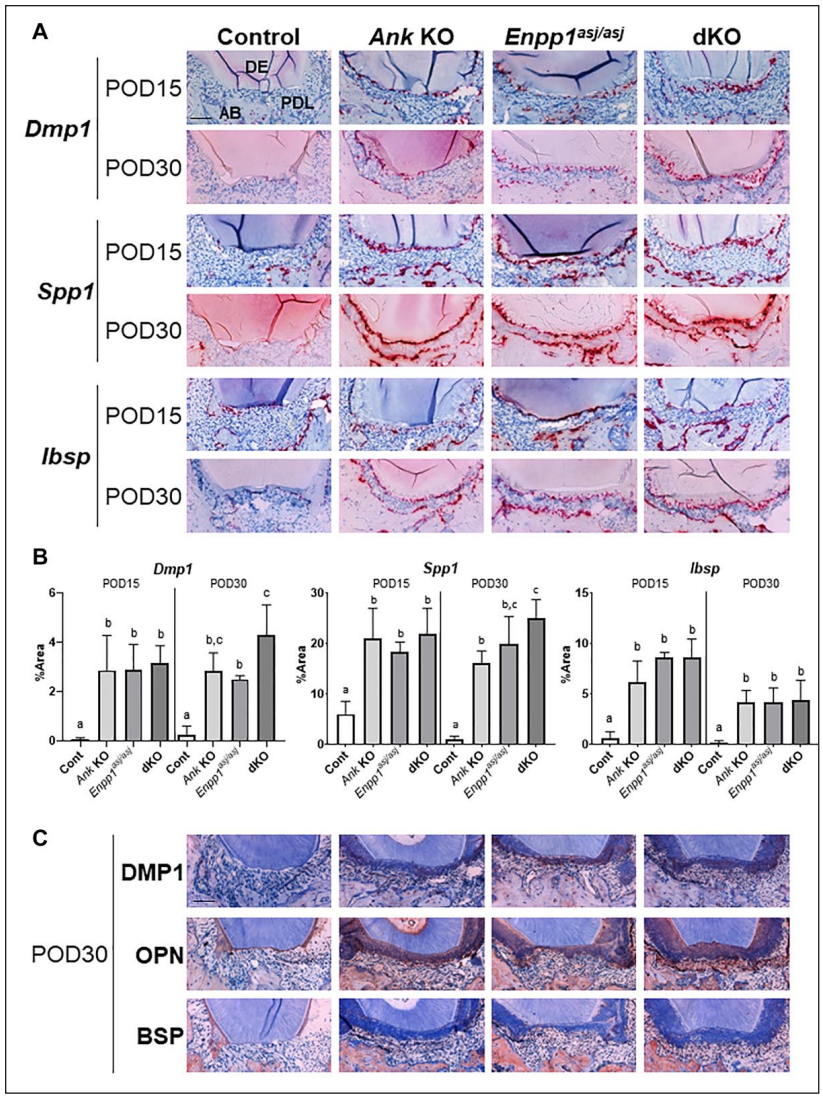

Figure 2. Increased expression of cementum markers coincides with increased cementogenesis in knockout (KO) and double knockout (dKO) mice. Representative images of (**A**) in situ hybridization (ISH) and (**C**) immunohistochemistry (IHC) staining for dentin matrix protein (*Dmp1*/DMP1), osteopontin (*Spp1*/OPN), and bone sialoprotein (*Ibsp*/BSP) at postoperative day (POD) 15 and POD30 ($n = 4$ per genotype). Single KOs and dKO mice exhibited greater expression and localization of all markers in association with cementum regeneration. AB, alveolar bone; DE, dentin; PDL, periodontal ligament. Scale bar: 50 µm. (**B**) Statistical analyses of ISH staining. All 3 markers are increased in regenerated cementum of all KO models versus controls at both POD15 and POD30 (*Dmp1: Ank* KO: 40-fold, 11-fold; *Enpp1*$^{asj/asj}$: 40-fold, 10-fold; dKO: 44-fold, 16-fold; *Spp1: Ank* KO: 3-fold, 17-fold; *Enpp1*$^{asj/asj}$: 3-fold, 21-fold; dKO: 4-fold, 27-fold; *Ibsp: Ank* KO: 10-fold, 22-fold; *Enpp1*$^{asj/asj}$: 13-fold, 21-fold; dKO: 13-fold, 22-fold, respectively, $P < 0.01$). At POD30, *Dmp1* and *Spp1* expression levels were significantly increased in dKO versus *Enpp1*$^{asj/asj}$ and *Ank* KO mice, respectively (1.7-fold and 1.5-fold, respectively, $P < 0.05$). Experimental groups marked by different letters (a, b, or c) within POD15 or POD30 are significantly different ($P < 0.05$, by one-way analysis of variance), while groups sharing the same letter are not different ($P > 0.05$).

threshold. The osteoid volume was significantly increased in dKO versus control mice at POD15 (3-fold, $P < 0.01$), with similar trends in single KO mice, but differences between genotypes were not observed at POD30 (Fig. 3C). Regenerated alveolar bone density showed an inverse trend compared to osteoid volume at POD30, with *Enpp1*$^{asj/asj}$ and dKO mice exhibiting decreased bone mineral density versus controls at POD30, while a similar trend was observed in *Ank* KO mice (6%, $P < 0.05$; 9%, $P < 0.01$, respectively) (Fig. 3D).

Regenerated bone was analyzed by ISH and IHC using established markers. In contrast to minimal expression of *Dmp1*/DMP1, *Spp1*/OPN, and *Ibsp*/BSP in cementum of control mice, expression levels for all markers were robust in regenerating alveolar bone of control mice at both POD15 and POD30, suggesting the process of bone regeneration was more active than cementum regeneration (Fig. 4). In all mice, *Dmp1* localized primarily to osteocytes within the bone matrix and DMP1 to osteocyte perilacunar matrix, while *Spp1* and *Ibsp* localized to osteoblasts on the surface and OPN and BSP immunolabeled throughout the regenerated bone (Fig. 4A, C). Quantitative measurement of ISH staining confirmed these 3 markers were significantly increased in regenerated bone of all 3 KO models versus controls at POD30 ($P < 0.05$). At POD15, *Dmp1* was significantly increased in dKO versus control (6-fold, $P < 0.05$), while a trend was observed in single KOs. *Ibsp* was significantly increased in all 3 KO models ($P < 0.001$), with no significant difference observed for *Spp1* (Fig. 4B). Some differences were observed between single KO and dKO at POD15 and POD30. *Spp1* at POD30 and *Ibsp* at POD15 were significantly increased in dKO versus *Ank* KO (1.4-fold and 1.3-fold, respectively, $P < 0.05$), and *Ibsp* POD30 was increased in dKO versus single KOs (2-fold, $P < 0.01$). IHC staining showed increased immunostaining for BSP, OPN, and DMP1 in alveolar bone matrix at POD30. In control mice, in contrast to other markers that were expressed in bone at both POD15 and POD30, *Spp1* was strongly expressed at POD15 with lower expression at POD30. These differences in the expression pattern of OPN between KOs and control mice coincide with findings of increased osteoid volume in KOs versus controls (Fig. 3), suggesting a role for OPN in modulating bone remodeling.

Increased Osteoclast Numbers in Single KOs and dKO Mice

Decreased bone mineral density and altered IHC staining in *Enpp1*$^{asj/asj}$ and dKO mice at POD30 prompted us to examine osteoclasts at healing sites. TRAP staining revealed no differences in TRAP^{+} osteoclast numbers at POD15, but at POD30, all KO models featured increased osteoclasts versus controls ($P < 0.001$). Furthermore, dKO mice showed significantly

increased osteoclast numbers compared to *Enpp1*$^{asj/asj}$ mice (2-fold, $P < 0.05$) (Fig. 5A). IHC indicated the number of cathepsin K$^+$ cells was increased in all 3 KO models versus controls at both time points ($P < 0.05$). Moreover, dKO showed increased cathepsin K$^+$ cells versus single KOs at POD15 (vs. *Ank* KO: 1.5-fold; vs. *Enpp1*$^{asj/asj}$: 1.7-fold; $P < 0.01$).

Discussion

Previous studies, focused on defining the role of factors modulating P_i/PP_i during periodontal development, demonstrated that *Ank* KO, *Enpp1*$^{asj/asj}$, and dKO mice featured similarly increased cementum. Here, we asked whether altered PP_i regulation during wound healing would parallel developmental findings. Using a fenestration wound-healing model, we show that ablation of *Ank* or *Enpp1* increased reparative cementogenesis versus controls, including increased expression of mineralized tissue extracellular matrix markers. In contrast, loss of ANK or ENPP1 did not increase alveolar bone regeneration, leading to a transient increase in osteoid and decreased bone mineral density. Effects on cementum and osteoid formation from concurrent ANK and ENPP1 loss were additive. Notably, we observed increased numbers of TRAP$^+$ and cathepsin K$^+$ osteoclasts within the regenerated alveolar bone in all KO models versus control mice.

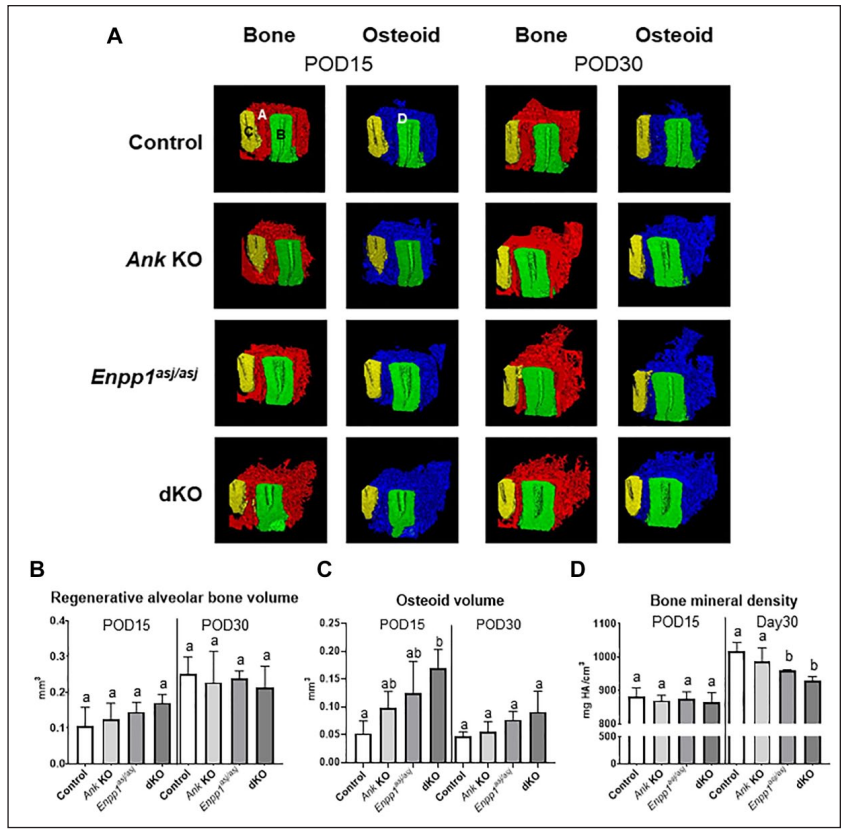

Figure 3. *Ank* and/or *Enpp1* ablation does not increase alveolar bone volume. (**A**) Representative micro-computed tomography (CT) images of regenerated mineralized alveolar bone (red) and osteoid (blue) ($n = 4$ per genotype). A (red), regenerated alveolar bone; B (green), distal root of first molar; C (yellow), mesial root of second molar; D (blue), partially mineralized osteoid. No differences between genotypes were found for (**B**) regenerated alveolar bone volume, but (**C**) partially mineralized osteoid volume was increased in double knockout (dKO) mice at postoperative day (POD) 15. (**D**) Bone mineral density was reduced in *Enpp1*$^{asj/asj}$ and dKO mice at POD30 (6%, $P < 0.05$ and 9%, $P < 0.01$, respectively). Experimental groups marked by different letters (a, b, or c) within POD15 or POD30 are significantly different ($P < 0.05$, by one-way analysis of variance), while groups sharing the same letter are not different ($P > 0.05$).

Reduction of PP_i Promotes Regeneration of Cementum

PP_i regulators, ANK and ENPP1, modulate cementogenesis and osteogenesis (Rodrigues et al. 2011; Foster et al. 2012; Thumbigere-Math et al. 2018; Chu et al. 2020). PP_i dysregulation has clear implications in humans and mice models. For example, individuals with generalized arterial calcification of infancy (GACI) exhibit hypercementosis due to loss of ENPP1 (Thumbigere-Math et al. 2018). Previous studies reported that *Enpp1*$^{asj/asj}$ mice have reduced serum PP_i levels (Albright et al. 2015), and loss of ANK resulted in intracellular PP_i accumulation and extracellular PP_i reduction (Ho et al. 2000). Furthermore, in vitro studies revealed 50% to 60% decreased extracellular PP_i in *Ank* KO versus WT primary osteoblasts (Harmey et al. 2004). In a proof-of-principle study, ANK loss of function promoted cementum regeneration (Rodrigues et al. 2011), and here we expand the scope to determine effects from ENPP1 loss and concurrent loss of ANK and ENPP1. All KO models in this study demonstrated accelerated and increased cementum regeneration versus controls. Differences were noted in response between *Ank* KO and *Enpp1*$^{asj/asj}$ mice (i.e., *Enpp1*$^{asj/asj}$ mice showed increased cementum thickness compared to *Ank* KO mice at POD30). Notably, developmentally there were no differences in cementum thicknesses between all KO models, suggesting that during development, there is a limit to the effects of PP_i on cementogenesis (Chu et al. 2020). In regeneration, ENPP1 loss of function has a more potent effect than ANK ablation. Moreover, dKO mice showed significantly increased regenerated cementum versus single KOs, suggesting additive effects of ANK and ENPP1. Factors beyond the P_i/PP_i ratio may be contributing to this effect, warranting further investigation.

Regenerated cementum in all KOs exhibited robust expression of mineralized tissue extracellular matrix markers, *Dmp1, Spp1*, and *Ibsp*, coinciding with increased cementum thickness. There appeared to be a trend of increased BSP in all KOs versus controls, but differences were not as clear as with ISH, confirming previous studies (Foster et al. 2011; Rodrigues

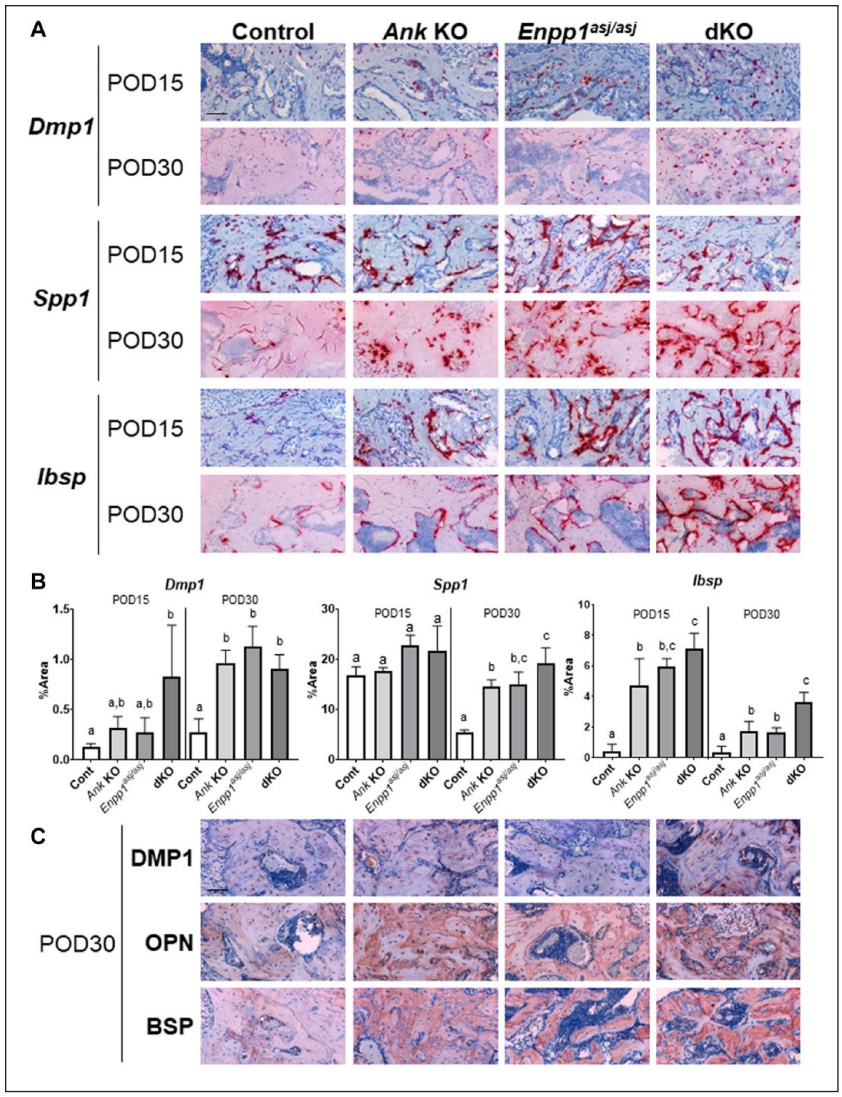

Figure 4. Increased expression of alveolar bone markers in knockout (KO) and double knockout (dKO) mice. Representative images of (**A**) in situ hybridization (ISH) and (**C**) immunohistochemistry (IHC) staining for dentin matrix protein (*Dmp1*/DMP1), osteopontin (*Spp1*/OPN), and bone sialoprotein (*Ibsp*/BSP) at postoperative day (POD) 15 and POD30 ($n = 4$ per genotype). Single KOs and dKO mice exhibited greater expression and localization of all markers in association with alveolar bone regeneration. Scale bar: 50 µm. (**B**) Statistical analyses of ISH staining. At POD15, *Ibsp* was significantly increased in all 3 KOs versus controls (*Ank* KO: 12-fold; *Enpp1*$^{asj/asj}$: 15-fold; dKO: 15-fold, $P < 0.001$). Although *Dmp1* was increased in dKO (6-fold, $P < 0.05$) with a similar trend in single KOs and no difference was observed in *Spp1* at POD15, all 3 markers were significantly increased in regenerated alveolar bone of all KO models versus controls at POD30 (*Dmp1: Ank* KO: 4-fold; *Enpp1*$^{asj/asj}$: 4-fold; dKO: 3-fold; *Spp1: Ank* KO: 6-fold; *Enpp1*$^{asj/asj}$: 5-fold; dKO: 9-fold; *Ibsp: Ank* KO: 5-fold; *Enpp1*$^{asj/asj}$: 5-fold; dKO: 11-fold, $P < 0.05$). *Spp1* at POD30 and *Ibsp* at POD15 were significantly increased in dKO versus *Ank* KO (1.4-fold and 1.3-fold, respectively, $P < 0.05$). *Ibsp* in dKO at POD30 was significantly increased versus single KOs (2-fold, $P < 0.01$). Experimental groups marked by different letters (a, b, or c) within POD15 or POD30 are significantly different ($P < 0.05$, by one-way analysis of variance), while groups sharing the same letter are not different ($P > 0.05$).

et al. 2011). In addition to serving as cementum markers, increased expression of these ECM proteins confirms previous studies demonstrating that modulators of P_i/PP_i levels affect expression of DMP1, OPN, and BSP (Addison et al. 2007; Foster et al. 2012; Nishino et al. 2017).

We and others demonstrated that PP_i regulation of cementogenesis is evolutionarily conserved across species, including mouse models of ANK, ENPP1, and TNAP loss-of-function and individuals with *ENPP1* or *ALPL* loss-of-function mutations (Foster et al. 2012; Zweifler et al. 2015; Thumbigere-Math et al. 2018; Chavez et al. 2020), supporting PP_i modulation as a novel approach to promote cementum regeneration. Backing this concept, we reported that pharmacologic manipulation of PP_i through an ENPP1-Fc fusion protein regulates cementum growth (Chu et al. 2020). Previous findings bolstered by new data here support further studies of therapeutic interventions targeting PP_i metabolism.

Altered Alveolar Bone Regeneration Associated with Reduced PP_i

Although reduced levels of PP_i promoted cementum regeneration, alveolar bone did not exhibit a similar regenerative response. These findings are not surprising because during wound healing, alveolar bone is in an active phase of formation and resorption, while cementum exhibits limited remodeling (Kusumbe et al. 2014). Critical processes in bone formation include osteoblast-mediated deposition of collagen-rich osteoid ECM, which mineralizes to form an ossification center (Kenkre and Bassett 2018). We noted increased osteoid volume at POD15 in dKO versus controls with a trend in single KOs, but by POD30, no differences were noted in osteoid volume between any of the phenotypes. No differences in bone volume were observed between phenotypes at POD15 or POD30. The initial increase in osteoid volume suggests delayed mineralization at early stages of regeneration. While speculative, this may be related to limited levels of PP_i at the regenerative site. In this regard, hyperosteoidosis with hypomineralization of other tissues has been linked with inadequate P_i/PP_i metabolism (Cundy et al. 2015; Kamiya et al. 2017). Further evidence of perturbed mineralization includes increased ectopic calcifications and reduced femur length in *Ank, Enpp1* dKO versus single KO mice (Harmey et al. 2004; Chu et al. 2020). In the appendicular skeleton, osteopenia in adult *Enpp1* KO mice is exacerbated over time, suggesting that ENPP1 loss alters bone remodeling (Mackenzie et al. 2012). Increased osteoid may also be related to increased *Spp1*/OPN

expression in regenerating alveolar bone of all KOs. OPN is considered an inhibitor of mineralization (Hunter et al. 1994; Boskey et al. 2002; Harmey et al. 2006). Decreased expression of *Spp1*/OPN at POD30 in control mice may reflect normal healing. In contrast, all KOs continued to exhibit strong expression of *Spp1*/OPN at POD30, suggesting OPN may affect bone remodeling, perhaps related to decreased levels of PP_i at sites of healing. Past studies suggest comparable effects of increased OPN expression in impairment of the mineralization process (Boskey et al. 2002; Harmey et al. 2006; Barros et al. 2013; Narisawa et al. 2013). Such a local response, if transient as would be expected with a local delivery of a regeneration factor, may prove to be beneficial (e.g., may slow down remodeling and thereby promote increased mineral formation fostered by the increased osteoid).

The altered regenerated bone profile in these animal models prompted us to assess osteoclast activity. Existing data from in vivo and in vitro models indicate that differentiation processes of osteoblasts and osteoclasts are influenced by P_i/PP_i ratio (Beck et al. 2000; Hayashibara et al. 2007; Nishino et al. 2017). Osteoclast differentiation markers (i.e., TRAP and cathepsin K) (Zhao et al. 2007) were significantly increased in all 3 KOs versus control. Furthermore, dKO mice showed increased number of $TRAP^+$ cells versus *Enpp1*$^{asj/asj}$ and cathepsin K^+ cells versus both single KOs. During development, *Ank* KO, *Enpp1*$^{asj/asj}$, and dKO mice also exhibited increased $TRAP^+$ osteoclasts on alveolar bone surfaces, but differences in bone mineral density were not detected between KO models and controls (Chu et al. 2020). These differences between bone formed during development versus wound healing indicate that in "challenge" models, loss of ANK and/or ENPP1 perturbs the balance between osteogenesis and osteoclastogenesis, which can lead to reduced mineral density. Previous studies focused on ANK support a role for this factor in modulating osteoblastic-osteoclastic homeostasis (Kim et al. 2010). It is intriguing to speculate that additional events related to wound healing may contribute to osteoclast function and further signify nonredundant roles for ANK and ENPP1.

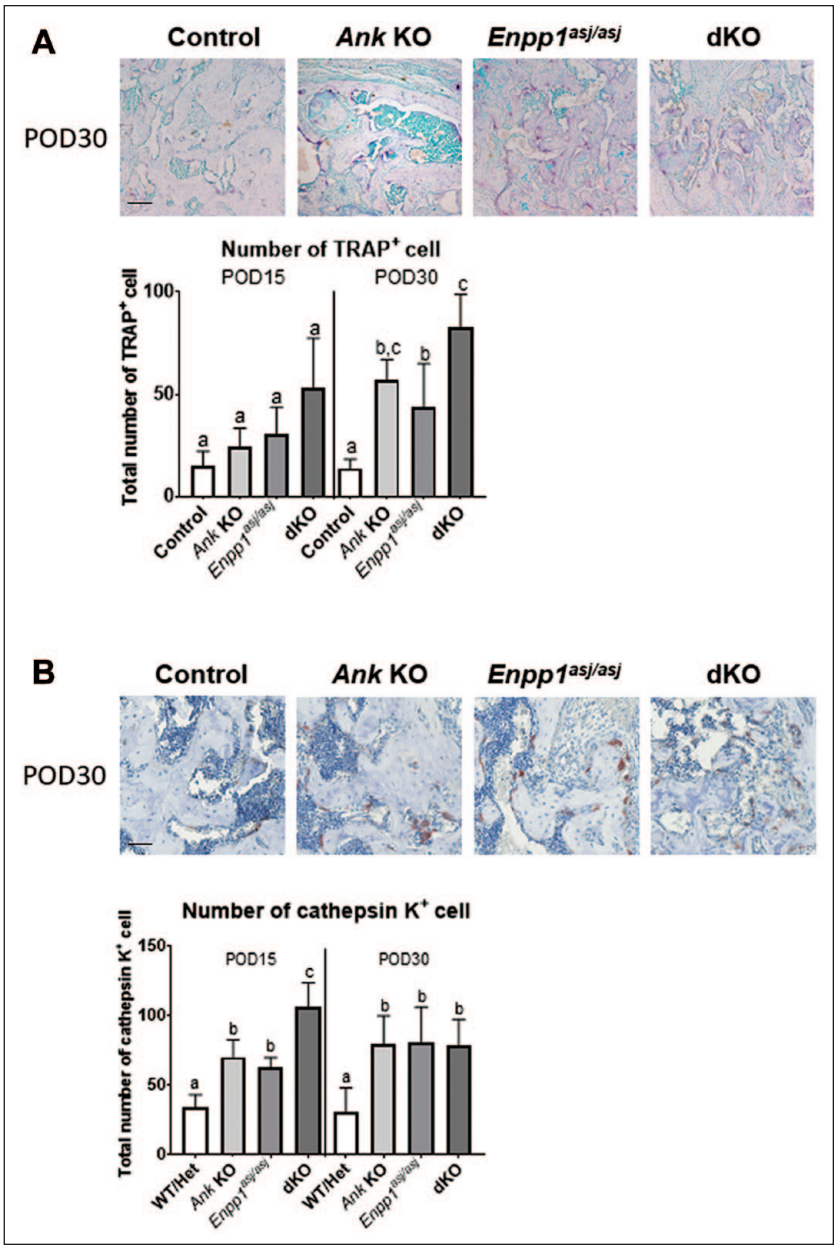

Figure 5. Increased osteoclast numbers in alveolar bone of knockout (KO) and double knockout (dKO) mice. (**A**) Representative images of tartrate-resistant acid phosphatase (TRAP) staining in all genotypes at postoperative day (POD) 30 ($n = 4$ per genotype). Scale bar: 50 µm. Increased numbers of $TRAP^+$ osteoclasts were localized to regenerated alveolar bone in *Ank* KO, *Enpp1*$^{asj/asj}$, and dKO versus control mice at POD30 (*Ank* KO: 4-fold, $P < 0.01$; *Enpp1*$^{asj/asj}$: 3-fold, $P < 0.05$; dKO: 6-fold, $P < 0.001$). Increased $TRAP^+$ osteoclasts were observed in dKO versus *Enpp1*$^{asj/asj}$ (2-fold, $P < 0.05$). (**B**) Representative immunohistochemistry (IHC) images for cathepsin K in all genotypes at POD30 ($n = 4$ per genotype). Scale bar: 50 µm. The number of cathepsin K^+ osteoclasts was significantly increased in all KO models versus controls at both POD15 (*Ank* KO: 2-fold, $P < 0.01$; *Enpp1*$^{asj/asj}$: 1.8-fold, $P < 0.05$; dKO: 3-fold, $P < 0.0001$) and POD30 (*Ank* KO, *Enpp1*$^{asj/asj}$, dKO: 3-fold, $P < 0.05$); furthermore, dKO showed more increased cathepsin K^+ osteoclasts versus single KOs at POD15 (vs. *Ank* KO: 1.5-fold; vs. *Enpp1*$^{asj/asj}$: 1.7-fold, $P < 0.01$). Experimental groups marked by different letters (a, b, or c) within POD15 or POD30 are significantly different ($P < 0.05$, by one-way analysis of variance), while groups sharing the same letter are not different ($P > 0.05$).

Our results emphasize mechanistic differences between cementum and bone regeneration, possibly attributable to high sensitivity of cementogenesis to alterations in PP_i, in conjunction with limited remodeling. This serves as a reminder to consider tissue-specific responses during periodontal tissue regeneration. Taken together, our preclinical studies suggest PP_i modulation as a potential approach for cementum regeneration, but large animal studies must be completed to build on these findings.

Author Contributions

A. Nagasaki, K. Nagasaki, E.Y. Chu, B.L. Foster, M.J. Somerman, contributed to conception, design, data acquisition, analysis, and interpretation, drafted and critically revised the manuscript; B.D. Kear, contributed to design, data acquisition, and analysis, drafted and critically revised the manuscript; W.D. Tadesse, S.E. Ferebee, contributed to design, data acquisition, and analysis, drafted the manuscript; L. Li, contributed to data acquisition, drafted the manuscript. All authors gave final approval and agree to be accountable for all aspects of the work.

Acknowledgments

We thank Dr. Francisco Nociti (State University of Campinas, Brazil) for assistance with fenestration defect surgical techniques, Dr. Renny Franceschi (University of Michigan) for providing polyclonal rabbit anti-mouse bone sialoprotein antibody, Dr. Vardit Kram for assistance with micro-CT scanning (National Institute of Dental and Craniofacial Research/NIH), and Dr. Davide Randazzo, Dr. Evelyn Ralston, and Ms. Aster Kinea (Light Imaging Section, National Institute of Arthritis and Musculoskeletal and Skin Diseases/NIH) for assistance in slide scanning.

Declaration of Conflicting Interests

The authors declared no potential conflicts of interest with respect to the research, authorship, and/or publication of this article.

Funding

The authors disclosed receipt of the following financial support for the research, authorship, and/or publication of this article: This work was funded by NIAMS Intramural Research Program, Japan Society for the Promotion of Science (JSPS) to A. Nagasaki (JSPS-NIH Research Fellow, JSPS Research Fellowship for Japanese Biomedical and Behavioral Researchers at NIH), K99/R00 grant AR073926 to E.Y. Chu, and R03DE028411 and R01DE027639 from National Institute of Dental and Craniofacial Research/NIH to B.L. Foster.

ORCID iDs

A. Nagasaki https://orcid.org/0000-0002-7655-9658
B.L. Foster https://orcid.org/0000-0003-3444-0576

References

Addison WN, Azari F, Sorensen ES, Kaartinen MT, McKee MD. 2007. Pyrophosphate inhibits mineralization of osteoblast cultures by binding to mineral, up-regulating osteopontin, and inhibiting alkaline phosphatase activity. J Biol Chem. 282(21):15872–15883.

Albright RA, Stabach P, Cao W, Kavanagh D, Mullen I, Braddock AA, Covo MS, Tehan M, Yang G, Cheng Z, et al. 2015. ENPP1-Fc prevents mortality and vascular calcifications in rodent model of generalized arterial calcification of infancy. Nat Commun. 6:10006.

Ao M, Chavez MB, Chu EY, Hemstreet KC, Yin Y, Yadav MC, Millan JL, Fisher LW, Goldberg HA, Somerman MJ, et al. 2017. Overlapping functions of bone sialoprotein and pyrophosphate regulators in directing cementogenesis. Bone. 105:134–147.

Barros NM, Hoac B, Neves RL, Addison WN, Assis DM, Murshed M, Carmona AK, McKee MD. 2013. Proteolytic processing of osteopontin by PHEX and accumulation of osteopontin fragments in Hyp mouse bone, the murine model of X-linked hypophosphatemia. J Bone Miner Res. 28(3):688–699.

Beck GR Jr, Zerler B, Moran E. 2000. Phosphate is a specific signal for induction of osteopontin gene expression. Proc Natl Acad Sci USA. 97(15):8352–8357.

Boskey AL, Spevak L, Paschalis E, Doty SB, McKee MD. 2002. Osteopontin deficiency increases mineral content and mineral crystallinity in mouse bone. Calcif Tissue Int. 71(2):145–154.

Bosshardt DD. 2005. Are cementoblasts a subpopulation of osteoblasts or a unique phenotype? J Dent Res. 84(5):390–406.

Chande S, Bergwitz C. 2018. Role of phosphate sensing in bone and mineral metabolism. Nat Rev Endocrinol. 14(11):637–655.

Chavez MB, Kramer K, Chu EY, Thumbigere-Math V, Foster BL. 2020. Insights into dental mineralization from three heritable mineralization disorders. J Struct Biol. 212(1):107597.

Chu EY, Vo TD, Chavez MB, Nagasaki A, Mertz EL, Nociti FH, Aitken SF, Kavanagh D, Zimmerman K, Li X, et al. 2020. Genetic and pharmacologic modulation of cementogenesis via pyrophosphate regulators. Bone. 136:115329.

Cundy T, Michigami T, Tachikawa K, Dray M, Collins JF, Paschalis EP, Gamsjaeger S, Roschger A, Fratzl-Zelman N, Roschger P, et al. 2015. Reversible deterioration in hypophosphatasia caused by renal failure with bisphosphonate treatment. J Bone Miner Res. 30(9):1726–1737.

Eke PI, Zhang X, Lu H, Wei L, Thornton-Evans G, Greenlund KJ, Holt JB, Croft JB. 2016. Predicting periodontitis at state and local levels in the United States. J Dent Res. 95(5):515–522.

Foster BL, Nagatomo KJ, Bamashmous SO, Tompkins KA, Fong H, Dunn D, Chu EY, Guenther C, Kingsley DM, Rutherford RB, et al. 2011. The progressive ankylosis protein regulates cementum apposition and extracellular matrix composition. Cells Tissues Organs. 194(5):382–405.

Foster BL, Nagatomo KJ, Nociti FH Jr, Fong H, Dunn D, Tran AB, Wang W, Narisawa S, Millan JL, Somerman MJ. 2012. Central role of pyrophosphate in acellular cementum formation. PLoS One. 7(6):e38393.

Foster BL, Popowics TE, Fong HK, Somerman MJ. 2007. Advances in defining regulators of cementum development and periodontal regeneration. Curr Top Dev Biol. 78:47–126.

Harmey D, Hessle L, Narisawa S, Johnson KA, Terkeltaub R, Millan JL. 2004. Concerted regulation of inorganic pyrophosphate and osteopontin by akp2, enpp1, and ank: an integrated model of the pathogenesis of mineralization disorders. Am J Pathol. 164(4):1199–1209.

Harmey D, Johnson KA, Zelken J, Camacho NP, Hoylaerts MF, Noda M, Terkeltaub R, Millan JL. 2006. Elevated skeletal osteopontin levels contribute to the hypophosphatasia phenotype in Akp2(−/−) mice. J Bone Miner Res. 21(9):1377–1386.

Hayashibara T, Hiraga T, Sugita A, Wang L, Hata K, Ooshima T, Yoneda T. 2007. Regulation of osteoclast differentiation and function by phosphate: potential role of osteoclasts in the skeletal abnormalities in hypophosphatemic conditions. J Bone Miner Res. 22(11):1743–1751.

Ho AM, Johnson MD, Kingsley DM. 2000. Role of the mouse ank gene in control of tissue calcification and arthritis. Science. 289(5477):265–270.

Hunter GK, Kyle CL, Goldberg HA. 1994. Modulation of crystal formation by bone phosphoproteins: structural specificity of the osteopontin-mediated inhibition of hydroxyapatite formation. Biochem J. 300(Pt 3):723–728.

Kamiya N, Yamaguchi R, Aruwajoye O, Kim AJ, Kuroyanagi G, Phipps M, Adapala NS, Feng JQ, Kim HK. 2017. Targeted disruption of NF1 in osteocytes increases FGF23 and osteoid with osteomalacia-like bone phenotype. J Bone Miner Res. 32(8):1716–1726.

Kassebaum NJ, Bernabe E, Dahiya M, Bhandari B, Murray CJ, Marcenes W. 2014. Global burden of severe periodontitis in 1990–2010: a systematic review and meta-regression. J Dent Res. 93(11):1045–1053.

Kenkre JS, Bassett J. 2018. The bone remodelling cycle. Ann Clin Biochem. 55(3):308–327.

Kim HJ, Minashima T, McCarthy EF, Winkles JA, Kirsch T. 2010. Progressive ankylosis protein (ANK) in osteoblasts and osteoclasts controls bone formation and bone remodeling. J Bone Miner Res. 25(8):1771–1783.

King GN, King N, Cruchley AT, Wozney JM, Hughes FJ. 1997. Recombinant human bone morphogenetic protein-2 promotes wound healing in rat periodontal fenestration defects. J Dent Res. 76(8):1460–1470.

Kusumbe AP, Ramasamy SK, Adams RH. 2014. Coupling of angiogenesis and osteogenesis by a specific vessel subtype in bone. Nature. 507(7492): 323–328.

Mackenzie NC, Zhu D, Milne EM, van't Hof R, Martin A, Quarles DL, Millan JL, Farquharson C, MacRae VE. 2012. Altered bone development and an increase in FGF-23 expression in Enpp1(−/−) mice. PLoS One. 7(2):e32177.

Millan JL. 2006. Alkaline phosphatases: structure, substrate specificity and functional relatedness to other members of a large superfamily of enzymes. Purinergic Signal. 2(2):335–341.

Narisawa S, Yadav MC, Millan JL. 2013. In vivo overexpression of tissue-nonspecific alkaline phosphatase increases skeletal mineralization and affects the phosphorylation status of osteopontin. J Bone Miner Res. 28(7): 1587–1598.

Nishino J, Yamazaki M, Kawai M, Tachikawa K, Yamamoto K, Miyagawa K, Kogo M, Ozono K, Michigami T. 2017. Extracellular phosphate induces the expression of dentin matrix protein 1 through the FGF receptor in osteoblasts. J Cell Biochem. 118(5):1151–1163.

Nociti FH Jr, Berry JE, Foster BL, Gurley KA, Kingsley DM, Takata T, Miyauchi M, Somerman MJ. 2002. Cementum: a phosphate-sensitive tissue. J Dent Res. 81(12):817–821.

Orriss IR, Arnett TR, Russell RG. 2016. Pyrophosphate: a key inhibitor of mineralisation. Curr Opin Pharmacol. 28:57–68.

Rodrigues TL, Nagatomo KJ, Foster BL, Nociti FH, Somerman MJ. 2011. Modulation of phosphate/pyrophosphate metabolism to regenerate the periodontium: a novel in vivo approach. J Periodontol. 82(12):1757–1766.

Rutsch F, Ruf N, Vaingankar S, Toliat MR, Suk A, Hohne W, Schauer G, Lehmann M, Roscioli T, Schnabel D, et al. 2003. Mutations in ENPP1 are associated with 'idiopathic' infantile arterial calcification. Nat Genet. 34(4):379–381.

Szeri F, Lundkvist S, Donnelly S, Engelke UFH, Rhee K, Williams CJ, Sundberg JP, Wevers RA, Tomlinson RE, Jansen RS, et al. 2020. The membrane protein ANKH is crucial for bone mechanical performance by mediating cellular export of citrate and ATP. PLoS Genet. 16(7):e1008884.

Thumbigere-Math V, Alqadi A, Chalmers NI, Chavez MB, Chu EY, Collins MT, Ferreira CR, FitzGerald K, Gafni RI, Gahl WA, et al. 2018. Hypercementosis associated with ENPP1 mutations and GACI. J Dent Res. 97(4):432–441.

Wolf M, Ao M, Chavez MB, Kolli TN, Thumbigere-Math V, Becker K, Chu EY, Jager A, Somerman MJ, Foster BL. 2018. Reduced orthodontic tooth movement in Enpp1 mutant mice with hypercementosis. J Dent Res. 97(8):937–945.

Yamamoto T, Li M, Liu Z, Guo Y, Hasegawa T, Masuki H, Suzuki R, Amizuka N. 2010. Histological review of the human cellular cementum with special reference to an alternating lamellar pattern. Odontology. 98(2):102–109.

Zhao Q, Shao J, Chen W, Li YP. 2007. Osteoclast differentiation and gene regulation. Front Biosci. 12:2519–2529.

Zweifler LE, Patel MK, Nociti FH Jr, Wimer HF, Millan JL, Somerman MJ, Foster BL. 2015. Counter-regulatory phosphatases TNAP and NPP1 temporally regulate tooth root cementogenesis. Int J Oral Sci. 7(1):27–41.